Published in final edited form as:

Cell Rep. 2024 August 27; 43(8): 114641. doi:10.1016/j.celrep.2024.114641.

Non-canonical autophosphorylation of RIPK1 drives timely pyroptosis to control *Yersinia* infection

David Jetton[1], **Hayley I. Muendlein**[2], **Wilson M. Connolly**[2], **Zoie Magri**[1], **Irina Smirnova**[2], **Rebecca Batorsky**[3], **Joan Mecsas**[4], **Alexei Degterev**[5], **Alexander Poltorak**[1,2,6,*]

[1]Graduate Program in Immunology, Tufts Graduate School of Biomedical Sciences, Boston, MA 02111, USA

[2]Department of Immunology, Tufts University School of Medicine, Boston, MA 02111, USA

[3]Data Intensive Studies Center, Tufts University, Medford, MA 02155, USA

[4]Department of Molecular Biology and Microbiology, Tufts University School of Medicine, Boston, MA 02111, USA

[5]Department of Cell, Molecular & Developmental Biology, Tufts University School of Medicine, Boston, MA 02111, USA

[6]Lead contact

SUMMARY

Caspase-8-dependent pyroptosis has been shown to mediate host protection from *Yersinia* infection. For this mode of cell death, the kinase activity of receptor-interacting protein kinase 1 (RIPK1) is required, but the autophosphorylation sites required to drive caspase-8 activation have not been determined. Here, we show that non-canonical autophosphorylation of RIPK1 at threonine 169 (T169) is necessary for caspase-8-mediated pyroptosis. Mice with alanine in the T169 position are highly susceptible to *Yersinia* dissemination. Mechanistically, the delayed formation of a complex containing RIPK1, ZBP1, Fas-associated protein with death domain (FADD), and caspase-8 abrogates caspase-8 maturation in T169A mice and leads to the eventual activation of RIPK3-dependent necroptosis *in vivo*; however, this is insufficient to protect the host, suggesting that timely pyroptosis during early response is specifically required to control infection. These results position RIPK1 T169 phosphorylation as a driver of pyroptotic cell death critical for host defense.

In brief

*Correspondence: alexander.poltorak@tufts.edu.

AUTHOR CONTRIBUTIONS

Conceptualization, A.P. and D.J.; validation, D.J., H.I.M., and W.M.C.; formal analysis, D.J. and A.D.; investigation, D.J., H.I.M., Z.M., A.D., and W.M.C.; writing, J.M., A.P., and D.J.; visualization, D.J.; supervision, A.P. and D.J.; project administration, A.P.; funding acquisition, A.P. and A.D.

DECLARATION OF INTERESTS

The authors declare no competing interests.

SUPPLEMENTAL INFORMATION

Supplemental information can be found online at https://doi.org/10.1016/j.celrep.2024.114641.

The role of specific autophosphorylations driving RIPK1-dependent death is unclear. Jetton et al. demonstrate that autophosphorylation of RIPK1 T169 is required to initiate caspase-8-dependent pyroptosis in response to *Yersinia* but is dispensable for death complex assembly or activating necroptosis, positioning RIPK1 T169 as critical for host defense from *Yersinia*.

Graphical Abstract

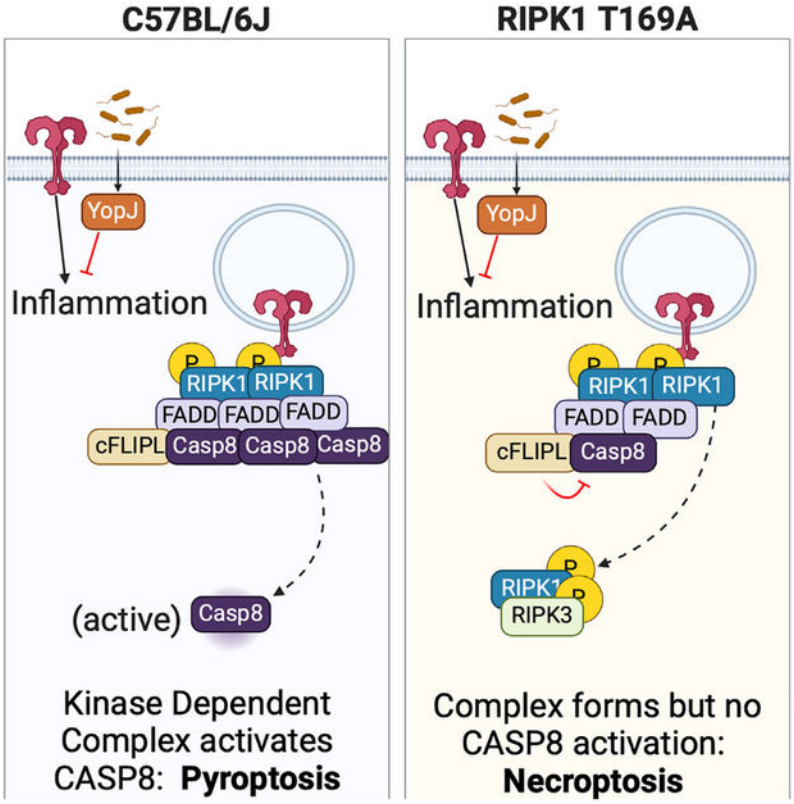

INTRODUCTION

Receptor-interacting protein kinase 1 (RIPK1) is a key regulator determining the cellular fate of innate immune cells during bacterial infection, balancing inflammatory signaling and cell death.[1–5] During infection, RIPK1 is recruited downstream of tumor necrosis factor (TNF) receptor as well as Toll-like receptors (TLRs) 3 and 4, where it acts as a poly-ubiquitinated scaffold leading to the transcription of cytokines, chemokines, and other pro-survival factors critical for the activation of the immune response.[6] To circumvent the host inflammatory response, many successful pathogens have evolved strategies to inhibit these host signaling cascades to establish a niche for their replication and survival.[7–10] In response, RIPK1 is released from the pro-inflammatory complex and becomes an active kinase available to drive the formation of various pro-death complexes that have been extensively characterized in recent years.[4,5,11] One of these kinase-dependent complexes recruits Fas-associated protein with death domain (FADD) and caspase-8 (CASP8) to drive CASP8-dependent apoptosis and pyroptosis. If unbound from CASP8, RIPK1 recruits another member of RIPK

family, RIPK3, that phosphorylates mixed-lineage kinase-like pseudokinase (MLKL) to drive RIPK3-dependent necroptosis.[4,5,11,12] In each of these complexes, the kinase activity of RIPK1 is exclusively engaged in autophosphorylation, with no *trans*-targets identified to date. Multiple studies using pharmacological inhibitors have identified RIPK1 kinase-dependent death as critical to control bacterial dissemination by inducing pro-inflammatory signaling in uninfected bystanders and eliminating the bacterial survival niche.[3,13,14] For this reason, the dual roles of RIPK1 in cell death and inflammation are highly regulated and vital host responses to infection.

Yersinia species are a group of gram-negative extracellular bacteria that induce disease in humans ranging from forms of gastroenteritis (*Y. pseudotuberculosis* and *Y. enterocolitica*) to plague (*Y. pestis*).[10,15] To inhibit the antibacterial inflammatory host response, *Yersinia* species utilize a type III secretion system to inject several *Yersinia* outer proteins (Yops), whose broad goals are to inhibit cytosolic processes.[1,10,16] One of them, YopJ, inhibits the kinase activity of transforming growth factor β activating kinase 1 (TAK1) via acetylation, causing the downregulation of multiple mitogen-activated protein kinases (MAPKs) downstream of TAK1 such as c-Jun N-terminal kinase, p38, and extracellular signal-regulated kinases 1 and 2, thereby inhibiting the activation of the downstream nuclear factor κB (NF-κB) and MAPK signaling cascades responsible for pro-inflammatory cytokine production and phagocyte recruitment.[2,7,17,18] In response to this pathogen-imposed inhibition, the affected macrophages downregulate ubiquitination of RIPK1, promoting the interaction of RIPK1 with FADD and CASP8 and leading to the activation of CASP8, cleavage of gasdermin D (GSDMD), and initiation of pyroptosis, a lytic form of cell death that is accompanied by the release of interleukin-1β (IL-1β).[4,5] Because of this, RIPK1 kinase-inactive mice that are unable to properly assemble the death complex are more susceptible to *Yersinia* infection.[1,2,11]

Despite our understanding of the kinase activity of RIPK1 as a key contributor in driving cell death and antimicrobial defense, the exact sequence and function of each of its kinase-specific phosphorylation events remain unclear. What is known is that several autophosphorylation sites are associated with cell death in the mouse, including serine residues 14/15, 161, and 166 and threonine 169.[14,19–23] It is also established that these phosphorylations work in concert to induce the conformational changes that allow for the oligomerization necessary to recruit downstream cell death effectors.[24] Autophosphorylation of S166 has long been held as the canonical biomarker of RIPK1 kinase activity, and reports have established the importance of this event in efficient complex formation to drive apoptosis or necroptosis.[20,25–30] However, the functional role of other autophosphorylation sites remains elusive. In extension of our previous work showing that lipopolysaccharide (LPS)-induced pyroptosis is driven by the RIPK1 kinase-dependent non-canonical activation of CASP8, here, we have utilized CRISPR-Cas9 technology and mass spectrometry to identify that T169 phosphorylation of RIPK1 is a critical event mediating cell death after infection with *Yersinia*. To relate this finding to the physiological context, we engineered a mouse with a T169 substitution on alanine and challenged them with *Yersinia pseudotuberculosis* (*Y.ptb*.). Excitingly, we report that loss of this phosphosite does not inhibit death complex assembly but rather inhibits the ability of the cell to activate caspases, thus leaving the host to have a greater susceptibility to YopJ-sufficient *Y.ptb*.

RESULTS

Phosphorylation of RIPK1 T169, and not canonical S166, drives cell death after stimulation with a model of *Yersinia*

We and others have previously reported that RIPK1 kinase activity is central in CASP8-dependent pyroptosis downstream of TLR4 driven by *Yersinia* species bacteria.[1,2,4,5] In this and other RIPK1-dependent modes of cell death, the kinase activity of RIPK1 drives autophosphorylation of several residues.[14,21] While RIPK1 S166 phosphorylation is the well-established biomarker of RIPK1 kinase activity, it has only been definitively shown to play a role in kinase-dependent apoptosis and necroptosis.[14,21,25,26,30,31] However, previous work from our lab has identified a model of RIPK1 kinase-dependent pyroptosis that does not upregulate the phosphorylation of RIPK1 S166.[32] This finding, together with the requirement for RIPK1 kinase activity, provided rationale for determining the phosphosite of RIPK1 that drives CASP8-dependent pyroptosis in the context of *Yersinia*-induced cell death. To gain support for this inquiry, we utilized immortalized bone marrow-derived macrophages (iBMDMs) and CRIPSR-Cas9 to generate two knockin RIPK1 mutant cell lines, one with substitution of serine at position 166 with alanine (RIPK1 S166A)[21] and one with substitution of aspartic acid at position 138 with asparagine (RIPK1 D138N kinase inactive) from the endogenous RIPK1 genomic locus (Figures S1A and S1B).[13] With these iBMDMs, we utilized LPS in combination with the inhibitor of TAK1, 5Z-7-oxozeaenol (5z7) as a model of YopJ-sufficient-*Yersinia*-induced death.[4,32–34] Accordingly, we found that S166A substitution in RIPK1 in iBMDMs resulted in an approximately 1-h delay in the initiation of death kinetics compared to B6, but these cells quickly reached a similar extent of nearly 80%–100% death. Conversely, the RIPK1 D138N kinase-inactive iBMDMs showed a much greater delay in the kinetics and extent of death, initiating death 4 h after the B6 and reaching a maximum of 40%–50% death (Figure 1A). This suggests that other residues of RIPK1 targeted by its kinase activity must have an important contribution to LPS/5z7-induced death. Because of the pyroptotic nature of LPS/5z7-induced cell death,[4,5] we compared the release of IL-1β in D138N and S166A iBMDMs by priming them with LPS to allow for the upregulation of pro-IL-1β followed by 5z7 treatment to induce death. In agreement with requirement of the kinase activity of RIPK1 for pyroptosis, IL-1β release was significantly reduced in the RIPK1 D138N iBMDMs or with the use of necrostatin-1 (Nec-1), a small-molecule inhibitor of RIPK1 kinase activity (Figure 1B), when compared to B6 iBMDMs primed with LPS and treated with 5z7. In contrast, RIPK1 S166A iBMDMs exhibited levels of IL-1β in the supernatants remarkably similar to the B6 iBMDMs, further suggesting that a different target of RIPK1 kinase activity drives the release of IL-1β. Because both pyroptosis and IL-1β release in the RIPK1 S166A iBMDMs were similar to B6 iBMDMs, we sought to further characterize any differences in death effector activation between D138N and S166A iBMDMs in response to LPS/5z7 treatment. To this end, we performed a time course of LPS/5z7 stimulation and assessed the activation of several caspases, GSDMD cleavage, and RIPK3 and MLKL phosphorylation by immunoblot. There were no significant changes to CASP8, CASP3, or GSDMD activation in the RIPK1 S166A iBMDMs, though all three were delayed or inhibited in the RIPK1 D138N line. The largest change observed in the RIPK1 S166A mutant cells appeared to be that these cells were unable to undergo RIPK3-dependent necroptosis, evidenced by the loss of

RIPK3 phosphorylation and downstream phosphorylation of the canonical executioner of necroptosis, MLKL (Figure 1C). Taken together, the sensitivity of S166A iBMDMs to LPS/5z7 treatment, their ability to secrete IL-1β in response to LPS/5z7, and their activation of cell death effectors downstream of TLR4 suggest that autophosphorylation of S166 is not required for pyroptosis and IL-1β release after treatment with LPS/5z7 as a model of *Yersinia*.

Given that LPS/5z7-induced pyroptosis required the kinase activity of RIPK1 and loss of S166 phosphorylation was unable to inhibit this death significantly, we used an unbiased approach to determine other possible amino acids targeted by RIPK1. In addition to S166, the mouse RIPK1 has been shown to be auto-phosphorylated at serine residues 14/15 and 161 and threonine 169, with all of these events being strongly inhibited by the addition of RIPK1 inhibitor Nec-1[14] (Figure 1D). To determine if any of these phosphorylations may have a role in CASP8-dependent pyroptosis, we precipitated RIPK1 from the lysates of BMDMs stimulated with LPS or LPS/5z7 and analyzed RIPK1-specific precipitates by mass spectrometry. Accordingly, we identified an upregulation of T169 and S14 phosphorylation in the BMDMs treated with LPS/5z7 but not those treated with LPS alone. To further investigate the requirement of T169 for CASP8-mediated pyroptosis, we knocked in alanine instead of threonine at position 169 in the endogenous *Ripk1* genomic locus to generate the T169A iBMDM cell line (Figure S1C). Similar to D138N iBMDMs, T169A iBMDMs were highly protected from LPS/5z7-induced pyroptosis and showed a near complete ablation of the release of IL-1β, in full resemblance of the kinase-inactive phenotype (Figures 1E and 1F). Taken together, the *in vitro* analysis of the role of the T169 residue in CASP8-mediated pyroptosis strongly suggested that autophosphorylation at T169 is essential for pyroptosis, thus supporting further investigation of the role of T169 in the context of *Yersinia* infection.

Inhibition of RIPK1 T169 phosphorylation inhibits CASP8-dependent death and downstream pyroptosis without altering inflammatory signaling

To address the role of RIPK1 T169 autophosphorylation *in vivo*, we used a CRISPR-based approach to generate a knockin mouse line with the same substitution of RIPK1 T169A (Figure 2A; Figure S2A). *Ripk1*$^{T169A/T169A}$ (RIPK1 T169A) mice were born at the expected Mendelian frequency and reached adulthood without abnormal pathology, indicating that loss of phosphorylation of RIPK1 T169 does not interfere with development and homeostasis. We first sought to confirm that the RIPK1 T169A BMDMs showed similar inflammatory signatures to B6 and that this mutation did not alter its inflammatory scaffolding functions. B6 and RIPK1 T169A BMDMs showed similar kinetics of activation of MAPK signaling in response to LPS or TNF-α (Figure S2B) as well of IκBα degradation and phosphorylation of NF-κB p65 (Figures S2C and S2D). We then sought to analyze changes in transcription by stimulating B6 and RIPK1 T169A BMDMs with LPS or LPS/5z7 for 2 h and collecting RNA for bulk sequencing analysis. Sample-sample comparison shows extremely high correlation within treatment groups, indicating that genotype does not seem to be a major driver of changes in transcriptional response (Figure 2B). Principal-component analysis of the bulk sequencing shows samples primarily grouping by stimulation and not by genotype (Figure 2C). Taken together, these results indicate that the RIPK1 T169A mutation did not alter the role of RIPK1 in inflammatory signaling.

We next asked if RIPK1 T169A mutation would alter RIPK1 kinase-dependent cell death in primary cells treated with models of *Yersinia*. To this end, we began by generating mouse embryonic fibroblasts (MEFs) to model RIPK1 kinase-dependent cell death and stimulated them with LPS and 5z7 as well as TNF-α and 5z7. RIPK1 T169A primary MEFs showed similar levels of protection from LPS/5z7 compared to B6 MEFs with the addition of Nec-1 (Figure 2E). Surprisingly, RIPK1 T169A MEFs showed an even greater level of protection from TNF-α/5z7 than B6 MEFs treated with TNF-α/5z7/Nec-1, indicating that the loss of phosphorylation at T169 may protect these cells even more than kinase inhibition (Figure 2E). Further, while we saw no change in death after treatment with TNF-α and cycloheximide, we saw that the RIPK1 T169A MEFs exhibited a reduction of death kinetics after treatment with the apoptosis inducer TNF-α and secondary mitochondrial-derived activator of caspases (smac) mimetics[35] similar to that after the addition of Nec-1 (Figures S2E and S2F). However, the death we observed in RIPK1 T169A MEFs treated with TNF-α, smac mimetics, and zVAD, which classically induces necroptosis,[36] was significantly inhibited by the addition of RIPK3 inhibitor GSK'872, which implies that these cells are still capable of strongly activating RIPK3-dependent necroptosis (Figure S2G).

In vivo, *Yersinia* targets macrophages, and thus, we sought to understand the effect of this mutation on the target cells. We generated BMDMs from B6, RIPK1 T169A, and *Ripk1*$^{D138N/D138N}$ (RIPK1 D138N) mice, which express a catalytically inactive form of RIPK1[13] with LPS and 5z7. As expected, the RIPK1 D138N kinase-inactive BMDMs displayed delayed kinetics and increased viability compared to B6.[37] Strikingly, the RIPK1 T169A primary BMDMs showed an even greater level of protection from LPS/5z7 than the kinase-inactive cells (Figure 2F). A similar inhibition was observed in response to infection of BMDMs with *Y.ptb*. (Figure 2G), which was eliminated with the addition of zVAD (Figure 2H), indicating that the increase in viability was caspase dependent. These differences in death kinetics were dependent upon the expression of the bacterial effector YopJ (Figure 2I). Additionally, macrophages from either RIPK1 T169A or RIPK1 D138N kinase-inactive mice also showed a significant reduction of IL-1β release into the supernatant after either infection with *Y.ptb*. or priming with LPS followed by 5z7 when compared to B6 (Figure 2J), without showing differences in IκBα degradation and phosphorylation of NF-κB p65 (Figure 2K), indicating that this change was not due to inflammatory signaling but rather the activation and release of IL-1β via cell death. Taken together, these data show that the RIPK1 T169A mutation displays a strong inhibition of CASP8-dependent pyroptosis in models of *Yersinia* infection while maintaining the ability to activate RIPK3 in models of necroptosis *in vitro*.

RIPK1 T169A BMDMs form a delayed death complex but do not induce caspase cleavage

To further characterize the mechanism of RIPK1 T169A inhibition, we compared caspase activation in B6 and RIPK1 T169A BMDMs after treatment with LPS or LPS/5z7. B6 BMDMs showed cleavage of CASP8 and downstream effectors CASP3 and CASP7 after 2 and 3 h of LPS/5z7 stimulation; in contrast, RIPK1 T169A BMDMs showed a near complete loss of activation of CASP8 as well as CASP3 and CASP7 (Figure 3A). Given that maturation of CASP8 toward p18 requires self-cleavage via its oligomerization and complexing with FADD and RIPK1, we next assessed the formation of the death complex.

To this end, we treated BMDMs from B6, RIPK1 T169A, and RIPK1 D138N mice with LPS/5z7, used antibodies to precipitate the death complex via FADD, and performed immunoblots for the presence of RIPK1 in complex. Two hours after treatment, we observed RIPK1 in complex with FADD in B6 BMDMs, which was further supported by cleavage of RIPK1 in the inputs, indicative of partial activation of CASP8 in complex with the inactive caspase paralog $cFLIP_L$ (cellular FLICE-like inhibitory protein)[38] and CASP8 that was fully matured to p18 at 2 and 4 h (Figure 3B). In agreement with previous reports, RIPK1 D138N BMDMs showed no association of FADD and RIPK1, along with a nearly complete loss of the RIPK1-cleaved fragment and CASP8 activation (Figure 3B). Strikingly, RIPK1 T169A BMDMs showed decreased association of FADD and RIPK1 at 2 h but increased association at 4 h. This coincided with the formation of a cleaved RIPK1 fragment but did not result in cleavage and full activation of CASP8 to the p18 fragment (Figure 3B).

We also confirmed that similar kinetics of complex formation were present when these BMDMs were infected *in vitro* with *Y.ptb*. (Figure 3C). After 1 h of infection with *Y.ptb*., we observed RIPK1 in complex with FADD in B6 BMDMs. In the inputs, we saw cleavage of RIPK1 by CASP8 that was fully matured to p18 and activation of GSDMD to the pore-forming p30 fragment by 3 h (Figure 3C).[39] In agreement with our previous publications, this also coincided with recruitment of ZBP1 into this complex (Figure 3C).[33] RIPK1 D138N BMDMs showed no association of FADD and RIPK1 or ZBP1, along with a nearly complete loss of the RIPK1-cleaved fragment, CASP8 activation, or GSDMD cleavage (Figure 3C). RIPK1 T169A BMDMs showed delayed association of FADD with RIPK1 and ZBP1 at 3 h, which coincided with the formation of a cleaved RIPK1[38] but did not result in the cleavage and full activation of CASP8 to the p18 fragment (Figure 3C). Furthermore, RIPK1 T169A-infected cells were unable to form the active p30 fragment of GSDMD, indicating the inhibition of pyroptosis in these cells (Figure 3C). These data suggested that phosphorylation of T169 regulates the kinetics of complex formation, which appears to be the key to the non-canonical activation of CASP8 and execution of pyroptosis. Collectively, these results show that despite the ability to promote death complex formation, the T169A mutation confers a significant delay in interactions between FADD, ZBP1, and RIPK1, which ultimately inhibits downstream activation of CASP8 and cell death even after the successful formation of a FADD-ZBP1-RIPK1 death complex.

T169A mice are more susceptible to *Y.ptb. in vivo*, corresponding to a decrease in splenic IL-1β during early infection

Based on our *in vitro* data (Figure 2G), RIPK1 T169A macrophages are highly resistant to *Yersinia*-induced cytotoxicity compared to both wild-type and RIPK1 D138N kinase-inactive macrophages. Remarkably, this protection does not come at the expense of inhibiting death complex formation as in the case of the RIPK1 D138N allele. This offers a unique model in which we can determine whether attenuated activation of CASP8 in T169A mice is compensated by other modes of cell death *in vivo*, as has been shown previously in other models.[40] To that end, we intravenously challenged B6, RIPK1 T169A, and RIPK1 D138N mice with *Y.ptb*. and monitored them for survival using the loss of 15% of body mass as a threshold requiring humane euthanasia. Over 80% of B6 mice succumbed to *Y.ptb*. between 4 and 7 days after infection. Of these mice, 84.2% were sacrificed due

to 15% loss criterion, and 10.5% died prior to critical weight loss (Figures 4A and 4B). Interestingly, while RIPK1 T169A mice exhibited a very similar ratio of death by weight loss to B6 mice (Figure 4B), they were significantly more susceptible to *Y.ptb*. infection (Figure 4A), succumbing between 3 and 5 days after infection, suggesting that a lack of pyroptotic cell death and IL-1β production could be the reason for their susceptibility *in vivo*. RIPK1 D138N kinase-inactive mice were highly susceptible to infection, similar to RIPK1 T169A mice, and succumbed to it within 4 days (Figure 4A). In contrast, most of the RIPK1 D138N mice died before they reached 15% weight loss, which alluded to physiological differences in death between RIPK1 T169A and D138N mice (Figure 4B). Finally, the changes in survival were YopJ dependent, as B6, RIPK1 T169A, and D138N mice infected with YopJ-deficient *Yersinia* show no difference in survival, all succumbing to infection around day 5 (Figure 4C). Taken together, these data suggest that the delayed assembly of the pro-death complex and its inhibition of CASP8 maturation have a significant impact on susceptibility to *Yersinia*, similar to that of kinase-inactive mice, where all modes of RIPK1 kinase-dependent death are abrogated. These data further emphasize that the timing of death complex assembly is a key factor in host-pathogen interactions.

To further understand the susceptibility in the RIPK1 T169A animals, we compared bacterial titers (colony-forming units [CFUs]) in the liver and spleen, which are targets of bacterial dissemination over the first 3 days of infection. We saw that although all three genotypes had similar tissue CFUs at days 1 and 2, there was a significant increase in bacterial burden in the spleen and liver of both the RIPK1 D138N kinase-inactive and RIPK1 T169A mice 3 days after infection when compared to B6 mice (Figure 4D). To determine whether relatively high bacterial growth in T169A mice might be conferred by the low levels of cytokines required for the recruitment of phagocytic cells, we compared cytokine responses to *Yersinia* infection on day 2 immediately preceding the divergence in CFUs. In the livers of all mice on day 2, there was no significant change in cytokine production (Figure S3A). Except for a significant increase in the TNF-α production in the RIPK1 D138N kinase-inactive spleen, we did not observe significant changes in IL-1β, IL-6, or CXCL1 compared to B6 (Figure 4E; Figure S3B). In contrast, there was a significant decrease in IL-1β in the RIPK1 T169A mice compared to the B6 mice (Figure 4E). We also sought to determine what changes may be present in the spleens of these mice on day 3, when CFUs had diverged. We found that both the RIPK1 T169A and RIPK1 D138N mice had significantly elevated levels of CXCL1 in the spleen, while again, the RIPK1 T169A mice showed a slight reduction in IL-1β compared to the RIPK1 D138N mice (Figure S3C). Taken together, these data support a model in which failure to timely assemble complex II in RIPK1 T169A mice results in the relative resistance of their macrophages to YopJ-mediated pyroptosis, low production of the IL-1β necessary to mount a sufficient antibacterial response, and a failure of RIPK1 T169A mice to control *Yersinia* infection when compared to B6 mice as disease progresses.

RIPK1 T169A mice experience delayed onset of cell death in the spleen after early *Y.ptb*. foci formation that rapidly increases to levels similar to those seen in B6 mice

Due to the fact that RIPK1 T169A mice experience heightened bacterial burden and attenuated IL-1β release in their spleens, we focused on the spleen to examine the possibility of a correlation between cell death and bacterial foci formation during *Yersinia* infection. Utilizing a strain of *Y.ptb*. that expresses GFP, we first compared the total cell death in spleens from B6, RIPK1 T169A, and RIPK1 D138N mice across 3 days of infection using terminal deoxynucleotidyl transferase-mediated deoxyuridine triphosphate nick end labeling (TUNEL) staining. In B6 mice, there was no observation of GFP+ *Y.ptb*. foci in the B6 spleens until day 3 (Figure 5A). These same B6 spleens saw TUNEL+ staining on day 2, which preceded the formation of bacterial foci, and further expanded on day 3, where TUNEL+ staining was observed adjacent to GFP+ *Y.ptb*. (Figures 5A–5C). In the RIPK1 D138N spleens, GFP+ *Y.ptb*. foci became visible on day 2 and greatly increased in number on day 3 (Figure 5A). These mice never saw a significant increase in TUNEL+ cells on day 2 or 3 (Figures 5A–5C). In contrast, the RIPK1 T169A spleens showed a striking delay in TUNEL+ cells (Figure 5A). In these spleens, we observed a significant decrease in TUNEL+ cells on day 2 compared to the B6 spleens, followed by a large number of TUNEL+ cells visible on day 3, which was quite comparable to the number of TUNEL+ cells in B6 spleens. Interestingly, RIPK1 T169A spleens had GFP+ *Y.ptb*. foci visible on day 2 when TUNEL+ staining was delayed, and these foci greatly grew in size on day 3 adjacent to the newly upregulated TUNEL+ signal (Figures 5A–5C). Taken together, these data indicate that splenocytes of the RIPK1 T169A mice experience delayed cell death compared to B6 mice but significantly greater cell death than the RIPK1 D138N kinase-inactive mice. Nonetheless, the delay in cell death in RIPK1 T169A coincides with an increase in bacterial foci formation that implies that it is specifically the early cell death that restrains bacterial growth and that cell death that occurs after expansion of bacterial foci formation is insufficient to restrain further bacterial burden.

RIPK1 T169A mice activate *p*-MLKL, and not CASP8, in the spleen during *in vivo Y.ptb*. infection

Given that RIPK1 T169A BMDMs showed a near complete protection from LPS/5z7 *in vitro*, which correlated with the delay in TUNEL staining *in vivo*, it seemed important to determine how the T169 spleens were able to initiate cell death that was comparable to B6 spleens after 3 days of infection. To identify the mechanism of cell death and cells that were undergoing this cell death, we performed immunofluorescence staining of sections of spleens from uninfected mice and mice infected with *Y.ptb*. for 3 days for colocalization of cleaved CASP8 and either CD68 or Ly6G. As expected, B6 spleens showed strong colocalization of CASP8 with CD68, indicating that monocytes and macrophages in the spleens were activating CASP8. While the Ly6G stain did not strongly colocalize with the CASP8+ stain in the B6 spleens, we did observe an increase in Ly6G+ neutrophil recruitment and formation of neutrophil swarms[41] (Figures 6A–6C). Interestingly, neither the RIPK1 T169A or RIPK1 D138N spleens showed a significant increase in cleaved CASP8 staining (Figures 6A and 6B), indicating that the cell death we measured by TUNEL+ staining (Figure 6C) was CASP8 independent. We also did not observe neutrophil swarming in the RIPK1 T169A or RIPK1 D138N spleens, suggesting that the delay in cell

death negatively impacts neutrophil recruitment or activation (Figure 6A). To understand the mechanism of the death observed in the RIPK T169A mice, we looked for the activation of the effectors of pyroptosis and necroptosis in the spleen lysates from mice infected for 3 days with *Y.ptb*. Analysis of B6 spleens for CASP8 cleavage by means of western blot revealed an expected increase in CASP8 cleavage, suggesting the normal execution of CASP8-dependent death in these spleens (Figure 6D). Further, infected B6 mice showed an increase in phospho-RIPK3 and phospho-MLKL, indicating the activation of RIPK3-MLKL-dependent necroptosis (Figure 6D). In contrast, there was no appreciable activation of CASP8 in infected RIPK1 T169A spleens, suggesting that these mice did not activate CASP8-dependent pyroptosis (Figure 6D). However, we did observe an increase in phospho-RIPK3 and phospho-MLKL in the RIPK1 T169A spleens (Figure 6D), indicating a possible switch in the cell death mechanism from pyroptosis to necroptosis. We did not observe the cleavage of CASP8 or an increase in phospho-RIPK3 or phospho-MLKL in RIPK1 D138N kinase-inactive mice (Figure 6D). Taken together, these data emphasize the importance of early CASP8-dependent pyroptosis to the host control of dissemination of *Y.ptb. in vivo*; however, the ability for RIPK1 T169A mice to form a death complex may enable these cells to engage in delayed necroptosis, which is insufficient to protect these animals from increased susceptibility.

DISCUSSION

RIPK1 is a complex protein involved in both inflammation and cell death. In the context of *Yersinia* infection accompanied by bacterial effector inhibition of the host immune response, RIPK1 kinase-dependent cell death is beneficial to the host by limiting the replicative niche that otherwise facilitates bacterial dissemination. If dysregulated, this kinase-dependent cell death becomes detrimental and contributes to the pathogenesis of numerous inflammatory diseases. These examples highlight some of the many evolutionary pressures driving precise regulation of RIPK1 enzymatic activity, which makes our understanding of the precise molecular mechanisms of RIPK1 activation via autophosphorylation challenging. In further complication, RIPK1 deficiency is perinatally lethal.[42] Previous work has established the importance of canonical RIPK1 S166 phosphorylation in driving apoptosis and necroptosis in several autoinflammatory settings, making this residue a useful biomarker for RIPK1 kinase activity.[21] However, the loss of S166 phosphorylation provides only partial protection from *in vitro* cell death compared to kinase-inactive animals, raising a question regarding the roles of other autophosphorylation sites. Given the ability of canonical RIPK1 S166 phosphorylation to enhance death complex formation and RIPK1 kinase activity that further promotes autophosphorylation of other residues, such as T169,[21] one possible model could be *Yersinia*-induced phosphorylation of S166 driving complex formation that enhances autophosphorylation of T169 to initiate CASP8 activation. Future studies will need to assess how RIPK1 autophosphorylation sites work in concert in a physiological setting by generating mouse models with mutations of multiple sites in combination to unravel the mechanisms by which autophosphorylation regulates the activation of RIPK1 kinase-dependent cell death.

In the present study, we advance our understanding of these mechanisms regulating RIPK1 kinase-dependent death and the role of that death in the control of *Yersinia* infection.

Specifically, *in vitro* experiments revealed that RIPK1 T169 autophosphorylation is required for CASP8-dependent pyroptosis and that the loss of RIPK1 T169 phosphorylation delays the formation of the death complex but does not inhibit it entirely. *In vivo*, the formation of the death complex is likely responsible for driving subsequent necroptosis during persistent *Yersinia* infection. Such a possibility is supported by cell death observed from *in-vivo*-infected RIPK1 T169A spleens (Figure 5A) and phosphorylation of MLKL in *in-vitro*-infected T169A BMDMs (Figure 6D). Considering our findings that show that loss of phosphorylation via the RIPK1 T169A mutation nearly completely abolishes *Y.ptb*.-induced death *in vitro*, but delays death *in vivo*, further characterization of the molecular basis of this dichotomy is necessary. Yet, these results highlight that the timing of death complex assembly and non-canonical activation of CASP8 is critical for host protection. Given that the loss of early pyroptosis cannot be replaced by the activation of necroptosis in later stages of infection, this indicates that RIPK1 acts as a rheostat for the prompt initiation of cell death. The delay of early pyroptosis also coincides with the loss of the necessary swarming of neutrophils, thereby reducing their necessary antimicrobial functions.[15,37]

Of note, human and murine myeloid cells behave very differently in response to *Yersinia* infection. While pathogenic *Yersinia* are often used to study cell death in murine systems, human macrophages and neutrophils appear to be much more resistant to YopJ- or 5z7-induced cell death compared to their murine counterparts.[4,43,44] In fact, human peripheral blood mononuclear cell-derived macrophages treated with LPS/5z7 display greater resistance than even RIPK1 D138N kinase-inactive BMDMs, just like RIPK1 T169A BMDMs (Figure 2A).[4] This is of some interest, as RIPK1 T169 is a highly conserved residue from fish to apes, but like our $Ripk1^{T169A/T169A}$ mice, humans do not possess RIPK1 T169. The loss of this autophosphorylation and the similar responses to both *Y.ptb.* and LPS/5z7 *in vitro* may suggest that $Ripk1^{T169A/T169A}$ mice exhibit a more human-like response to Yersinia. The differential response of human and murine macrophages to *Yersinia* supports the need to further study both mouse and human cells to understand the course of illness in humans and suggests that $Ripk1^{T169A/T169A}$ mice may be ideally positioned for future investigation.

Limitations of the study

The authors recognize that the RIPK1 T169 autophosphorylation site does not exist in humans and generated the T169A mutant specifically to investigate the loss of the autophosphorylation, not to explore the role of the human residue RIPK1 N169. Further understanding of human autophosphorylations will need to be done in the future with this understanding. This study also utilized an intravenous injection of *Yersinia* that specifically bypasses the intestine to determine the effect that the RIPK1 T169A mutation has on macrophage function. Possible roles for the RIPK1 T169A mutation have not been assessed in models that assess a role for RIPK1 in the gut, and therefore, the inability for necroptosis to rescue the loss of CASP8-dependent pyroptosis may be dependent on the route of infection.

STAR★METHODS

RESOURCE AVAILABILITY

Lead contact—Requests for further information, resources and reagents should be directed to the lead contact, Alexander Poltorak (alexander.poltorak@tufts.edu).

Materials availability—Mouse line *Ripk1*$^{T169A/T169A}$ generated in this study will be available by request after the signing of an MTA from the corresponding author.

Data and code availability—All data reported in this paper will be shared by the lead contact upon request. This paper does not report original code. Any additional information required to reanalyze the data reported in this paper is available from the lead contact upon request.

EXPERIMENTAL MODEL AND SUBJECT DETAILS

Animals—Balb/c mice were obtained from The Jackson Laboratory for generation of BMDMs to run mass spectroscopy analysis. For all other experiments, C57BL/6J mouse strain was obtained from The Jackson Laboratory. mi*Ripk1* $^{D138N/D138N}$ mice were a generous gift from Dr. M.A. Kelliher (University of Massachusetts Medical School) and were generated in collaboration with Dr. M. Pasparakis (University of Cologne). All genetically modified mice were fully backcrossed to the C57BL/6 background. All mice were housed in a pathogen-free facility at the Tufts University School of Medicine and experiments were performed in accordance with regulations and approval of the Tufts University Institutional Animal Care and Use Committee.

CRISPR/Cas9-mediated generation of Ripk1$^{T169A/T169A}$ mice—For the generation of *Ripk1*$^{T169A/T169A}$ mice, S.p. Cas9 (IDT) together with the 120 bp ssDNA repair oligo (IDT) and the short guide RNA (sgRNA) *comprised of both crRNA and tracrRNA sequences* (IDT) were microinjected into the pronucleus of fertilized oocytes obtained from C57BL/6J mice by University of Massachusetts Medical School Transgenic Animal Modeling Core. A sgRNA targeting a site adjacent to position 169 of the murine Ripk1 gene was used (5′ GAC ATG GAG CAA ACT GAC TA3′). On the next day, the injected embryos were transferred to foster mothers and allowed to develop to term. Mutations in the genome of progeny were determined by analysis of genomic DNA by sequencing. The sequence of the ssDNA oligo used as repair template for the RIPK1 T169A knock-in was 5′ CGA TCT TGG TGT GGC TTC CTT TAA GAC ATG GAG CAA ACT GGC TAA GGA GAA AGA CAA CAA GCA GAA AGA AGT GAG CAG CAC CA 3’. Primers to amplify gDNA fragments for sequencing were: (5′ GGT TAT CTT TCT CTG CCT TTA TGT G 3′) and (5′ TGT CTT ACT CTC ATA GGG CTC C 3′). Mice containing the desired knock-in were backcrossed to C57BL/6J mice for 4 generations before progeny from separate founders were crossed to generate the homozygote Ripk1$^{T169A/T169A}$.

Mouse bone marrow derived macrophages (BMDMs)—Bone marrow was flushed from femurs of indicated mouse strains with cold RPMI. Isolated cells were pelleted and re-suspended in BMDM differentiating media (RPMI with L-glutamine, 20% FBS, 30%

L-cell conditioned media, 2% Pen-Strep) and cultured for 7 days at 37°C in 5% CO2 to differentiate. Matured BMDMs were rested overnight in RPMI with L-glutamine 10% FBS, 2% Pen-Strep prior to experiments. *Yersinia* based experiments were conducted in the absence of antibiotics.

Generation of MEFs—C57Bl/6J or RIPK1 T169A mice were bred, and pregnancy was harvested between day 12.5–14.5 of gestation. Uterine horns were dissected, the embryo head and livers were removed, and individual embryos were homogenized and treated with trypsin and primary MEFs were cultured in high-glucose DMEM supplemented with 10% FBS, and 2% penicillin and streptomycin and allowed to reach 85% confluency before passage. At passage 3, primary MEFs were frozen for use in future experiments or plated directly for viability assays.

Yersinia pseudotuberculosis infection model—Prior to infection with *Y.ptb.*, mice were co-housed for at least two weeks. For survival studies, 8–10-week-old male and female C57Bl/6J, RIPK1 T169A, and RIPK1 D138N mice were injected intravenously with 5×10^2 colony forming units of *Yersinia pseudotuberculosis* IP2666 or *Yersinia pseudotuberculosis* IP2666 ΔYopJ in sterile PBS (100 μl), or equal volume of sterile PBS for control mice. Mice were monitored and temperature was monitored daily by rectal thermometer. When mouse body mass reached <85% of starting weight, mice were euthanized by CO_2 asphyxiation. For CFU, tissue collection, or tissue specific ELISA, C57Bl/6J, RIPK1 T169A, and RIPK1 D138N mice were injected intravenously with 5×10^2 colony forming units of *Yersinia pseudotuberculosis* IP2666 or *Yersinia pseudotuberculosis* IP2666 GFP+ in sterile PBS (100 μl), or equal volume of sterile PBS for control mice. Mice were monitored and temperature was monitored daily by rectal thermometer. At indicated timepoints after administration of *Y.ptb.*, or when mouse body mass reached <85% of starting weight, mice were euthanized by CO_2 asphyxiation, and tissue was collected for appropriate quantification. Tissue specific cytokines were analyzed at indicated timepoints after infection with Y.ptb IP2666. Tissues were weighed and single cell suspensions were generated in 0.5 mL PBS and cytokine secretion was measured by ELISA. Murine TNFα (DY410) and CXCL-1 (DY453) and IL-6 (DY406) and IL-1β (DY401) DuoSet ELISA kits were used according to the manufacturer's instructions. To determine bacterial burden, mice were euthanized at indicated timepoints and tissues were harvested, homogenized in 0.5 mL of PBS, and serially diluted on Luria–Bertani (LB) agar. All experiments were performed in accordance with regulations and approval of the Tufts University Institutional Animal Care and Use Committee.

Immortalized bone marrow derived macrophages (iBMDM)—Immortalized B6 BMDMs were a generous gift from Dr. K. Fitzgerald (University of Massachusetts Medical School) and were maintained in complete DMEM (DMEM with glucose, L-glutamine, 10% FBS, and 1% Pen-Strep).

CRISPR/Cas9-mediated generation of iBMDMs—For the generation of RIPK1 D138N, RIPK1 S166A, and RIPK1 T169A iBMDMs, Alt-R S.p. Cas9 Nuclease V3 (IDT, 1081058) together with Alt-R Cas9 Electroporation Enhancer (IDT, 1075915), Alt-R HDR Enhancer V2 (IDT, 10007910) the 80–120 bp ssDNA repair oligo (IDT) and the short guide

RNA (sgRNA) *comprised of both Alt-R CRISPR-Cas9 crRNA and tracrRNA sequences* (IDT) were nucleofected into B6 iBMDMs using the Nucleofector IIb system on program Y-001. Nucleofected cells were allowed to rest for 48 h, and single cell clones were grown in 96 well plates. Mutations in the clones were determined by analysis of genomic DNA by sequencing. To generate RIPK1 D138N sgRNA targeting a site adjacent to position 138 of the murine Ripk1 gene was used (5′ TGA CAA AGG TGT GAT ACA CA 3′). The sequence of the ssDNA oligo used as repair template for the RIPK1 D138N knock-in was 5′ ATA GAA GGC ATG TGC TAC TTA CAT GAC AAA GGT GTG ATA CAC AAG AAC CTG AAG CCT GAG AAT ATC CTC GTT GAT CGT GAC TTT CA 3’. To generate RIPK1 S166A sgRNA targeting a site adjacent to position 166 of the murine Ripk1 gene was used (5′ GAC ATG GAG CAA ACT GAC TA3′). The sequence of the ssDNA oligo used as repair template for the RIPK1 S166A knock-in was 5′ TCT TTT CCA GAT AGC CGA TCT TGG TGT GGC TTC CTT TAA GAC ATG GGC CAA ACT GAC TAA GGA GAA AGA CAA CAA GCA GAA AGA AGT GA 3’. To generate RIPK1 T169A sgRNA targeting a site adjacent to position 169 of the murine Ripk1 gene was used (5′ GAC ATG GAG CAA ACT GAC TA3′). The sequence of the ssDNA oligo used as repair template for the RIPK1 T169A knock-in was 5′ CGA TCT TGG TGT GGC TTC CTT TAA GAC ATG GAG CAA ACT GGC TAA GGA GAA AGA CAA CAA GCA GAA AGA AGT GAG CAG CAC CA 3’. Primers to amplify gDNA fragments for sequencing RIPK1 D138N were: (5′ TAT ATT TCA CCA TTT TCT CCT TCC C 3′) and (5′ GGA AAC AAA ACC CAG GAA CC 3′). Primers to amplify gDNA fragments for sequencing RIPK1 S166A and RIPK1 T169A were: (5′ GGT TAT CTT TCT CTG CCT TTA TGT G 3′) and (5′ TGT CTT ACT CTC ATA GGG CTC C 3′).

METHOD DETAILS

Reagents—LPS Escherichia coli 011: B4 (10 ng/mL for all BMDM assays and 100 ng/mL for all MEFs, L4391), 5z7 (125 nM, O9890), GSK’872(3 μM, 530389), and Nec-1 (10 μM, N9037) were purchased from Sigma- Aldrich.

Cell viability assays—MEFs were plated in tissue culture treated, 384-well, optical bottom plates (Nunc 142761) at 8.3×10^4 cells per well in DMEM with 10% FBS with 2% Pen-Strep. BMDMs were plated in tissue culture treated, 384-well, optical bottom plates (Nunc 142761) at 25×10^4 cells per well in RPMI with L-glutamine 10% FBS with or without 2% Pen-Strep. Indicated treatments were added to cells in media containing 10 μg/mL propidium iodide (Life Technologies, P3566). The Cytation3 Imager (BioTek) was used to maintain temperature at 37°C and 5% CO_2 during the experiments. Kinetic microscopy was performed by the Cytation3 Imager to quantify propidium iodide uptake every 30 min. Wells containing 0.1% Triton X-100 lysed cells were used as 100% cytotoxicity controls, and wells containing unstimulated cells were used as controls for baseline death overtime.

ELISA—1×10^5 BMDMs were plated on 96-well TC treated plates and stimulated as indicated for 16 h. LPS priming (10 ng/mL) occurred 4 h before the addition of 5z7 or nigericin, respectively. Cell free supernatants were analyzed for IL-1β (DY401) protein levels using the DuoSet ELISA kit from R&D Systems.

Mass spectrometry analysis—Balb/c BMDMs were treated as indicated for 30 min followed by IP of RIPK1. Eluted RIPK1 was run on a 4–15% Tris HCl gradient gel (BioRad, 3450028), visualized by Coomassie stain and sent to the laboratory of Dr. S. Gerber (Dartmouth University). RIPK1 was trypsinized and run on LS-MS/MS and peaks corresponding with phosphosites were identified.

Yersinia growth conditions—Wild-type IP2666 and ΔYopJ IP2666 *Y. pseudotuberculosis* bacterial strains were generously provided by R. Isberg. Bacteria were grown from frozen glycerol stocks on LB plates containing Irgasan (Sigma-Aldrich). Cultures were grown overnight in 2XYT broth at 26°C before addition of 200nM Sodium Oxalate and 2M $MgCl_2$ and cultured for 2 additional hours before a shift to 37°C for 2 h. Macrophages were infected at a multiplicity of infection (MOI) of 12 colony-forming units per cell.

Next generation sequencing—5×10^5 BMDMs were plated on 24-well TC treated plates and total RNA was isolated from unstimulated, LPS, and LPS/5z7 stimulated B6 BMDMs using TRIzol as recommended by the manufacturer. A TrueSeq kit was used to make a directional cDNA library. Seventy-five bp pair-end reads from cDNA libraries were generated on MiSeq (Illumina). Raw read data were trimmed to remove adapters using Trim Galore with default settings. Reads were aligned with STAR (reference GRCm39) using default settings. FeatureCounts counted raw read counts using gene annotation data from gencode M32. Differential gene expression between all pairs of conditions was performed with DESeq2 and plots were produced using ggplot R package.

Western blotting—Whole-cell lysates were prepared by lysing cells directly in 1X Laemmli Buffer with 5% β-mercaptoethanol. Tissue lysates were prepared by removing and weighing the tissue and generating single cell suspensions in PBS. Cell suspensions were lysed in 1X Laemmli Buffer with 5% β-mercaptoethanol at approximately 1 μg/μL final concentration. Samples were boiled for 15 min, followed by a 10-min incubation on ice. Protein lysates were resolved on a 10% or 15% Bis-Tris SDS gel and transferred to a nitrocellulose membrane using the Pierce Power transfer system. Membranes were blocked with 5% BSA in PBS-T for 1 h. Primary antibodies were diluted to 1:1000 in 1% BSA in PBS-T, and membranes were incubated with primary antibodies overnight at 4°C. Infrared secondary antibodies (680 or 700 nm) were diluted 1:30,000 in 1% BSA in PBS-T, and membranes were incubated with secondary antibodies for 40 min at room temperature. Membranes were imaged using an Odyssey CLx Imaging System, and image analysis was performed using Image Studio software.

FADD and RIPK1 immunoprecipitations—Cells were plated on 6 well TC treated plates, stimulated as indicated, and harvested in IP lysis buffer [0.5% Triton X-100, 50 mM Tris base (pH 7.4), 150 mM NaCl, 2 mM EDTA, 2 mM EGTA, and 1× protease inhibitor cocktail] as previously described.[47] Lysed cells were rotated for 60 min at 4°C with intermittent vortexing and centrifuged at 5000×g for 5 min, and the supernatant was incubated with α- FADD (Millipore Sigma, 05–048) or α- RIPK1 antibody (BD Biosciences, 610458) –conjugated Protein G–agarose beads (Cell Signaling Technology,

37478) overnight after removal of 10% of sample to be used as inputs. Samples were washed three times in IP lysis buffer, and protein complexes were eluted with 1× Laemmli buffer containing 5% β-mercaptoethanol at 90°C for 15 min.

TUNEL staining—For histology and TUNEL staining, spleens were isolated from GFP+ *Y.ptb*.- or PBS-injected mice after indicated timepoints, fixed in 4% paraformaldehyde in PBS (4%PFA) (Thermo Scientific, J19943-K2) for 4 h, and flash frozen in Tissue Plus O.C.T Compound (Fisher Scientific, 4585). Tissue sections were generated from frozen blocks by iHisto. Sections were fixed with 4% PFA for 20 min, washed with PBS, and permeabilized with 0.1% Triton in sodium citrate solution (Novus, NB900–62075). TUNEL staining was performed with *In Situ* Cell Death detection Kit, TMR red (Roche, 12156792910). Imaging and analysis of % TUNEL+ cells per field of view were calculated on the BioTek Lionheart Automated microscope. All experiments were performed in accordance with regulations and approval of the Tufts University Institutional Animal Care and Use Committee.

Histology and immunofluorescent staining—For histology and immunofluorescent staining, spleens were isolated from *Y.ptb*.- or PBS-injected mice after indicated timepoints, fixed in 10% formalin for 48 h, and transferred to 75% ethanol. Tissue sections were paraffin embedded by iHisto. Sections were deparaffinized with use of Xylene for 10 min and decreasing concentrations of ethanol in 3-min washes. Antigen retrieval was performed in sodium citrate buffer (Novus, NB900–62075) in a vegetable steamer for 20 min. Sections were washed in TBS plus 0.025% Triton X-100 and blocked in 10% normal serum and 1% BSA in TBS for 2 h. Primary antibodies were diluted at 1:250 in TBS with 1% BSA. Fluorophore conjugated secondary antibodies were diluted 1:100 in TBS with 1%BSA. All experiments were performed in accordance with regulations and approval of the Tufts University Institutional Animal Care and Use Committee.

QUANTIFICATION AND STATISTICAL ANALYSIS

For all *in vitro* experiments, mean values are presented +/− standard deviation. Error bars in ELISA experiments represent the standard deviation of three independent experiments. Data from kinetic cytotoxicity experiments and western blots are representative of 3 or more experiments, and error bars represent the standard deviation between triplicate samples. For *in vivo* experiments, values from individual mice are presented ($n \geq 4$), as well as mean values+/− standard deviation. two-way ANOVA was used for comparison between groups: ns, nonsignificant ($p > 0.05$); *$p < 0.05$; **$p < 0.01$; ***$p < 0.001$; ****$p < 0.0001$.

Supplementary Material

Refer to Web version on PubMed Central for supplementary material.

ACKNOWLEDGMENTS

We thank Dr. K. Fitzgerald for sharing immortalized BMDMs and Dr. M. Kelliher for sharing the *Ripk1*$^{D138N/D138N}$ mouse strain for this study. We thank Dr. R. Isberg for sharing the *Y. pseudotuberculosis* strains used in this study. We thank A. Tai and the Tufts University Genomics Core for help with RNA sequencing and data analysis. This work was supported by NIH grants AI167245 and AI056234 to A.P., AI144400 to A.D., and AI169782 to J.M.

REFERENCES

1. Peterson LW, Philip NH, DeLaney A, Wynosky-Dolfi MA, Asklof K, Gray F, Choa R, Bjanes E, Buza EL, Hu B, et al. (2017). RIPK1-dependent apoptosis bypasses pathogen blockade of innate signaling to promote immune defense. J. Exp. Med. 214, 3171–3182. [PubMed: 28855241]
2. Philip NH, Dillon CP, Snyder AG, Fitzgerald P, Wynosky-Dolfi MA, Zwack EE, Hu B, Fitzgerald L, Mauldin EA, Copenhaver AM, et al. (2014). Caspase-8 mediates caspase-1 processing and innate immune defense in response to bacterial blockade of NF-κB and MAPK signaling. Proc. Natl. Acad. Sci. 111, 7385–7390. [PubMed: 24799700]
3. Demarco B, Grayczyk JP, Bjanes E, Le Roy D, Tonnus W, Assenmacher CA, Radaelli E, Fettrelet T, Mack V, Linkermann A, et al. (2020). Caspase-8-dependent gasdermin D cleavage promotes antimicrobial defense but confers susceptibility to TNF-induced lethality. Sci. Adv. 6, eabc3465. [PubMed: 33208362]
4. Sarhan J, Liu BC, Muendlein HI, Li P, Nilson R, Tang AY, Rongvaux A, Bunnell SC, Shao F, Green DR, and Poltorak A (2018). Caspase-8 induces cleavage of gasdermin D to elicit pyroptosis during Yersinia infection. Proc. Natl. Acad. Sci. 115, E10888–E10897. [PubMed: 30381458]
5. Orning P, Weng D, Starheim K, Ratner D, Best Z, Lee B, Brooks A, Xia S, Wu H, Kelliher MA, and Berger SB (2018). Pathogen blockade of TAK1 triggers caspase-8–dependent cleavage of gasdermin D and cell death. Science 2818, 1064–1069.
6. Kelliher MA, Grimm S, Ishida Y, Kuo F, Stanger BZ, and Leder P (1998). The death domain kinase RIP mediates the TNF-induced NF-κB signal. Immunity 8, 297–303. [PubMed: 9529147]
7. Paquette N, Conlon J, Sweet C, Rus F, Wilson L, Pereira A, Rosadini CV, Goutagny N, Weber ANR, Lane WS, et al. (2012). Serine/threonine acetylation of TGFβ-activated kinase (TAK1) by Yersinia pestis YopJ inhibits innate immune signaling. Proc. Natl. Acad. Sci. USA 109, 12710–12715. [PubMed: 22802624]
8. Peltzer N, Darding M, and Walczak H (2016). Holding RIPK1 on the Ubiquitin Leash in TNFR1 Signaling. Trends Cell Biol. 26, 445–461. [PubMed: 26877205]
9. Mukherjee S, Keitany G, Li Y, Wang Y, Ball HL, Goldsmith EJ, and Orth K (2006). Yersinia YopJ Acetylates and Inhibits Kinase Activation by Blocking Phosphorylation. Science 312, 1211–1214. [PubMed: 16728640]
10. Viboud GI, and Bliska JB (2005). YERSINIA OUTER PROTEINS: Role in Modulation of Host Cell Signaling Responses and Pathogenesis. Annu. Rev. Microbiol. 59, 69–89. 10.1146/annurev.micro.59.030804.121320. [PubMed: 15847602]
11. Weng D, Marty-Roix R, Ganesan S, Proulx MK, Vladimer GI, Kaiser WJ, Mocarski ES, Pouliot K, Chan FKM, Kelliher MA, et al. (2014). Caspase-8 and RIP kinases regulate bacteria-induced innate immune responses and cell death. Proc. Natl. Acad. Sci. USA 111, 7391–7396. [PubMed: 24799678]
12. Degterev A, Ofengeim D, and Yuan J (2019). Targeting RIPK1 for the treatment of human diseases. Proc. Natl. Acad. Sci. USA 116, 9714–9722. [PubMed: 31048504]
13. Polykratis A, Hermance N, Zelic M, Roderick J, Kim C, Van TM, Lee TH, Chan FKM, Pasparakis M, and Kelliher MA (2014). Cutting Edge: RIPK1 Kinase Inactive Mice Are Viable and Protected from TNF-Induced Necroptosis In Vivo. J. Immunol. 193, 1539–1543. [PubMed: 25015821]
14. Degterev A, Hitomi J, Germscheid M, Ch'en IL, Korkina O, Teng X, Abbott D, Cuny GD, Yuan C, Wagner G, et al. (2008). Identification of RIP1 kinase as a specific cellular target of necrostatins. Nat. Chem. Biol. 4, 313–321. [PubMed: 18408713]
15. Hinnebusch BJ (2005). The Evolution of Flea-borne Transmission in Yersinia pestis. Curr. Issues Mol. Biol. 7, 197–212. [PubMed: 16053250]
16. Monack DM, Mecsas J, Ghori N, and Falkow S (1997). Yersinia signals macrophages to undergo apoptosis and YopJ is necessary for this cell death. Proc. Natl. Acad. Sci. USA 94, 10385–10390. [PubMed: 9294220]
17. Palmer LE, Pancetti AR, Greenberg S, and Bliska JB (1999). YopJ of Yersinia spp. is sufficient to cause downregulation of multiple mitogen-activated protein kinases in eukaryotic cells. Infect. Immun. 67, 708–716. [PubMed: 9916081]

18. Rosadini CV, Zanoni I, Odendall C, Green ER, Paczosa MK, Philip NH, Brodsky IE, Mecsas J, and Kagan JC (2015). A Single Bacterial Immune Evasion Strategy Dismantles Both MyD88 and TRIF Signaling Pathways Downstream of TLR4. Cell Host Microbe 18, 682–693. [PubMed: 26651944]
19. Berger SB, Kasparcova V, Hoffman S, Swift B, Dare L, Schaeffer M, Capriotti C, Cook M, Finger J, Hughes-Earle A, et al. (2014). Cutting Edge: RIP1 Kinase Activity Is Dispensable for Normal Development but Is a Key Regulator of Inflammation in SHARPIN-Deficient Mice. J. Immunol. 192, 5476–5480. [PubMed: 24821972]
20. Dondelinger Y, Delanghe T, Priem D, Wynosky-Dolfi MA, Sorobetea D, Rojas-Rivera D, Giansanti P, Roelandt R, Gropengiesser J, Ruckdeschel K, et al. (2019). Serine 25 phosphorylation inhibits RIPK1 kinase-dependent cell death in models of infection and inflammation. Nat. Commun. 10, 1729–1816. [PubMed: 30988283]
21. Laurien L, Nagata M, Schünke H, Delanghe T, Wiederstein JL, Kumari S, Schwarzer R, Corona T, Krüger M, Bertrand MJM, et al. (2020). Autophosphorylation at serine 166 regulates RIP kinase 1-mediated cell death and inflammation. Nat. Commun. 11, 1747. [PubMed: 32269263]
22. Delanghe T, Dondelinger Y, and Bertrand MJM (2020). RIPK1 Kinase-Dependent Death: A Symphony of Phosphorylation Events. Trends Cell Biol. 30, 189–200. [PubMed: 31959328]
23. Zhang Y, Su SS, Zhao S, Yang Z, Zhong CQ, Chen X, Cai Q, Yang ZH, Huang D, Wu R, and Han J (2017). RIP1 autophosphorylation is promoted by mitochondrial ROS and is essential for RIP3 recruitment into necrosome. Nat. Commun. 8, 14329. [PubMed: 28176780]
24. Wegner KW, Saleh D, and Degterev A (2017). Complex Pathologic Roles of RIPK1 and RIPK3: Moving Beyond Necroptosis. Trends Pharmacol. Sci. 38, 202–225. [PubMed: 28126382]
25. Zelic M, Pontarelli F, Woodworth L, Zhu C, Mahan A, Ren Y, LaMorte M, Gruber R, Keane A, Loring P, et al. (2021). RIPK1 activation mediates neuroinflammation and disease progression in multiple sclerosis. Cell Rep. 35, 109112. [PubMed: 33979622]
26. Ofengeim D, Ito Y, Najafov A, Zhang Y, Shan B, DeWitt JP, Ye J, Zhang X, Chang A, Vakifahmetoglu-Norberg H, et al. (2015). Activation of necroptosis in multiple sclerosis. Cell Rep. 10, 1836–1849. [PubMed: 25801023]
27. Jaco I, Annibaldi A, Lalaoui N, Wilson R, Tenev T, Laurien L, Kim C, Jamal K, Wicky John S, Liccardi G, et al. (2017). MK2 Phosphorylates RIPK1 to Prevent TNF-Induced Cell Death. Mol. Cell 66, 698–710.e5. [PubMed: 28506461]
28. Dondelinger Y, Delanghe T, Rojas-Rivera D, Priem D, Delvaeye T, Bruggeman I, Van Herreweghe F, Vandenabeele P, and Bertrand MJM (2017). MK2 phosphorylation of RIPK1 regulates TNF-mediated cell death. Nat. Cell Biol. 19, 1237–1247. [PubMed: 28920952]
29. Patel S, Webster JD, Varfolomeev E, Kwon YC, Cheng JH, Zhang J, Dugger DL, Wickliffe KE, Maltzman A, Sujatha-Bhaskar S, et al. (2020). RIP1 inhibition blocks inflammatory diseases but not tumor growth or metastases. Cell Death Differ. 27, 161–175. [PubMed: 31101885]
30. Ofengeim D, Mazzitelli S, Ito Y, DeWitt JP, Mifflin L, Zou C, Das S, Adiconis X, Chen H, Zhu H, et al. (2017). RIPK1 mediates a disease-associated microglial response in Alzheimer's disease. Proc. Natl. Acad. Sci. USA 114, E8788–E8797. [PubMed: 28904096]
31. Ofengeim D, and Yuan J (2013). Regulation of RIP1 kinase signalling at the crossroads of inflammation and cell death. Nat. Rev. Mol. Cell Biol. 14, 727–736. [PubMed: 24129419]
32. Muendlein HI, Jetton D, Connolly WM, Eidell KP, Magri Z, Smirnova I, and Poltorak A (2020). cFLIP L protects macrophages from LPS-induced pyroptosis via inhibition of complex II formation. Science 367, 1379–1384. [PubMed: 32193329]
33. Muendlein HI, Connolly WM, Magri Z, Smirnova I, Ilyukha V, Gautam A, Degterev A, and Poltorak A (2021). ZBP1 promotes LPS-induced cell death and IL-1β release via RHIM-mediated interactions with RIPK1. Nat. Commun. 12, 86. [PubMed: 33397971]
34. Wu J, Powell F, Larsen NA, Lai Z, Byth KF, Read J, Gu RF, Roth M, Toader D, Saeh JC, and Chen H (2013). Mechanism and in vitro pharmacology of TAK1 inhibition by (5 Z)-7-oxozeaenol. ACS Chem. Biol. 8, 643–650. [PubMed: 23272696]
35. Petersen SL, Wang L, Yalcin-Chin A, Li L, Peyton M, Minna J, Harran P, and Wang X (2007). Autocrine TNFα Signaling Renders Human Cancer Cells Susceptible to Smac-Mimetic-Induced Apoptosis. Cancer Cell 12, 445–456. [PubMed: 17996648]

36. He S, Wang L, Miao L, Wang T, Du F, Zhao L, and Wang X (2009). Receptor Interacting Protein Kinase-3 Determines Cellular Necrotic Response to TNF-α. Cell 137, 1100–1111. [PubMed: 19524512]
37. Chen KW, Demarco B, Ramos S, Heilig R, Goris M, Grayczyk JP, Assenmacher CA, Radaelli E, Joannas LD, Henao-Mejia J, et al. (2021). RIPK1 activates distinct gasdermins in macrophages and neutrophils upon pathogen blockade of innate immune signaling. Proc. Natl. Acad. Sci. USA 118, e2101189118. [PubMed: 34260403]
38. Pop C, Oberst A, Drag M, Van Raam BJ, Riedl SJ, Green DR, and Salvesen GS (2011). FLIPL induces caspase 8 activity in the absence of interdomain caspase 8 cleavage and alters substrate specificity. Biochem. J. 433, 447–457. [PubMed: 21235526]
39. He WT, Wan H, Hu L, Chen P, Wang X, Huang Z, Yang ZH, Zhong CQ, and Han J (2015). Gasdermin D is an executor of pyroptosis and required for interleukin-1beta secretion. Cell Res. 25, 1285–1298. [PubMed: 26611636]
40. Oberst A, Dillon CP, Weinlich R, McCormick LL, Fitzgerald P, Pop C, Hakem R, Salvesen GS, and Green DR (2011). Catalytic activity of the caspase-8-FLIP L complex inhibits RIPK3-dependent necrosis. Nature 471, 363–367. [PubMed: 21368763]
41. Shannon JG, Bosio CF, and Hinnebusch BJ (2015). Dermal Neutrophil, Macrophage and Dendritic Cell Responses to Yersinia pestis Transmitted by Fleas. PLoS Pathog. 11, e1004734. [PubMed: 25781984]
42. Dillon CP, Weinlich R, Rodriguez DA, Cripps JG, Quarato G, Gurung P, Verbist KC, Brewer TL, Llambi F, Gong YN, et al. (2014). RIPK1 blocks early postnatal lethality mediated by caspase-8 and RIPK3. Cell 157, 1189–1202. [PubMed: 24813850]
43. Spinner JL, Seo KS, O'Loughlin JL, Cundiff JA, Minnich SA, Bohach GA, and Kobayashi SD (2010). Neutrophils are resistant to Yersinia YopJ/P-induced apoptosis and are protected from ROS-mediated cell death by the type III secretion system. PLoS One 5, e9279. [PubMed: 20174624]
44. Wang JS, Wu D, Huang DY, and Lin WW (2015). TAK1 inhibition-induced RIP1-dependent apoptosis in murine macrophages relies on constitutive TNF-α signaling and ROS production. J. Biomed. Sci. 22, 1–13. [PubMed: 25563241]
45. Dobin A, Davis CA, Schlesinger F, Drenkow J, Zaleski C, Jha S, Batut P, Chaisson M, and Gingeras TR (2013). STAR: Ultrafast universal RNA-seq aligner. Bioinformatics 29, 15–21. [PubMed: 23104886]
46. Liao Y, Smyth GK, and Shi W (2014). FeatureCounts: An efficient general purpose program for assigning sequence reads to genomic features. Bioinformatics 30, 923–930. [PubMed: 24227677]
47. Siokas I, Zhang D, Poltorak A, Muendlein H, and Degterev A (2021). Immunoprecipitation Strategies to Isolate RIPK1/RIPK3 Complexes in Mouse Macrophages. Curr. Protoc. 1, e156. [PubMed: 34106523]

Highlights

- Autophosphorylation of RIPK1 T169 drives CASP8 activation in response to *Yersinia* infection
- A delay in death complex assembly in RIPK1 T169A mutant BMDMs abrogates CASP8 activation
- RIPK1 T169A mice switch from pyroptosis to necroptosis, which fails to protect from *Y.ptb*.

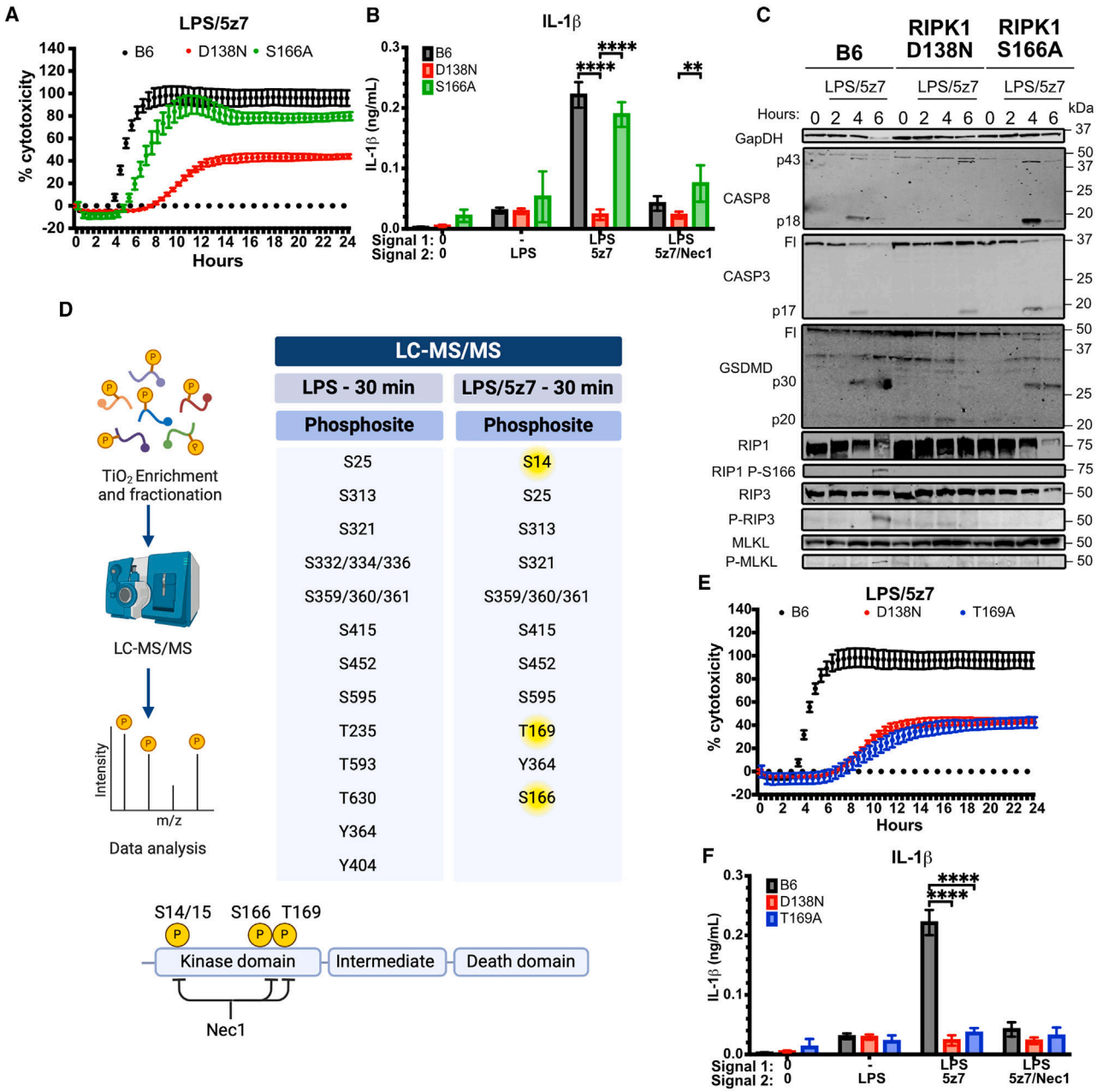

Figure 1. Phosphorylation of RIPK1 T169, and not canonical S166, drives cell death after stimulation with LPS/5z7

(A) Cell death as measured by propidium iodide (PI) incorporation over time in B6, RIPK1 S166A, and RIPK1 D138N knockin immortalized BMDMs stimulated with LPS/5z7.

(B) IL-1β release from B6, RIPK1 S166A, and RIPK1 D138N knockin immortalized BMDMs after 16 h of indicated treatments. LPS priming (10 ng/mL) occurred 4 h before the addition of 5z7 or 5z7/Nec-1.

(C) Western blot for GapDH, cleaved CASP8, CASP3, GSDMD, total RIPK1, phospho-S166 RIPK1, total RIPK3, phospho-RIPK3, total MLKL, and phospho-MLKL in LPS/5z7-stimulated B6, RIPK1 S166A, and RIPK1 D138N immortalized BMDMs stimulated with LPS/5z7 over the indicated amounts of time.

(D) Schema depicting workflow of phospho-specific mass spectroscopy. Phosphosites detected by liquid chromatography-tandem mass spectrometry (LC-MS/MS) in BMDMs treated with LPS or LPS/5z7 for 30 min. Previously reported autophosphorylations are highlighted in yellow and identified in the representation on the bottom. Schemas were created in BioRender.

(E) Cell death as measured by PI incorporation over time in B6, RIPK1 T169A, and RIPK1 D138N knockin immortalized BMDMs stimulated with LPS/5z7.

(F) IL-1β release from B6, RIPK1 S166A, and RIPK1 D138N knockin immortalized BMDMs after 16 h of indicated treatments. LPS priming (10 or 100 ng/mL) occurred 4 h before the addition of 5z7 or nigericin, respectively.</p/> Data from cell death assays and western blots are representative of 3 or more independent experiments, cell death data are presented as the mean ± SD of triplicate wells, and n = 10,000 cells examined in three individual wells. IL-1β release data are presented as the mean ± SD for triplicate wells from n = 3 independent experiments. Data from (A) and (E) as well as (B) and (F) were generated concurrently using the same B6 and D138N controls but are presented separately for narrative purposes. Two-way analysis of variance (ANOVA) was used for comparison between groups: ns, non-significant ($p > 0.05$), *$p < 0.05$, **$p < 0.01$, ***$p < 0.001$, and ****$p < 0.0001$.

See also Figure S1.

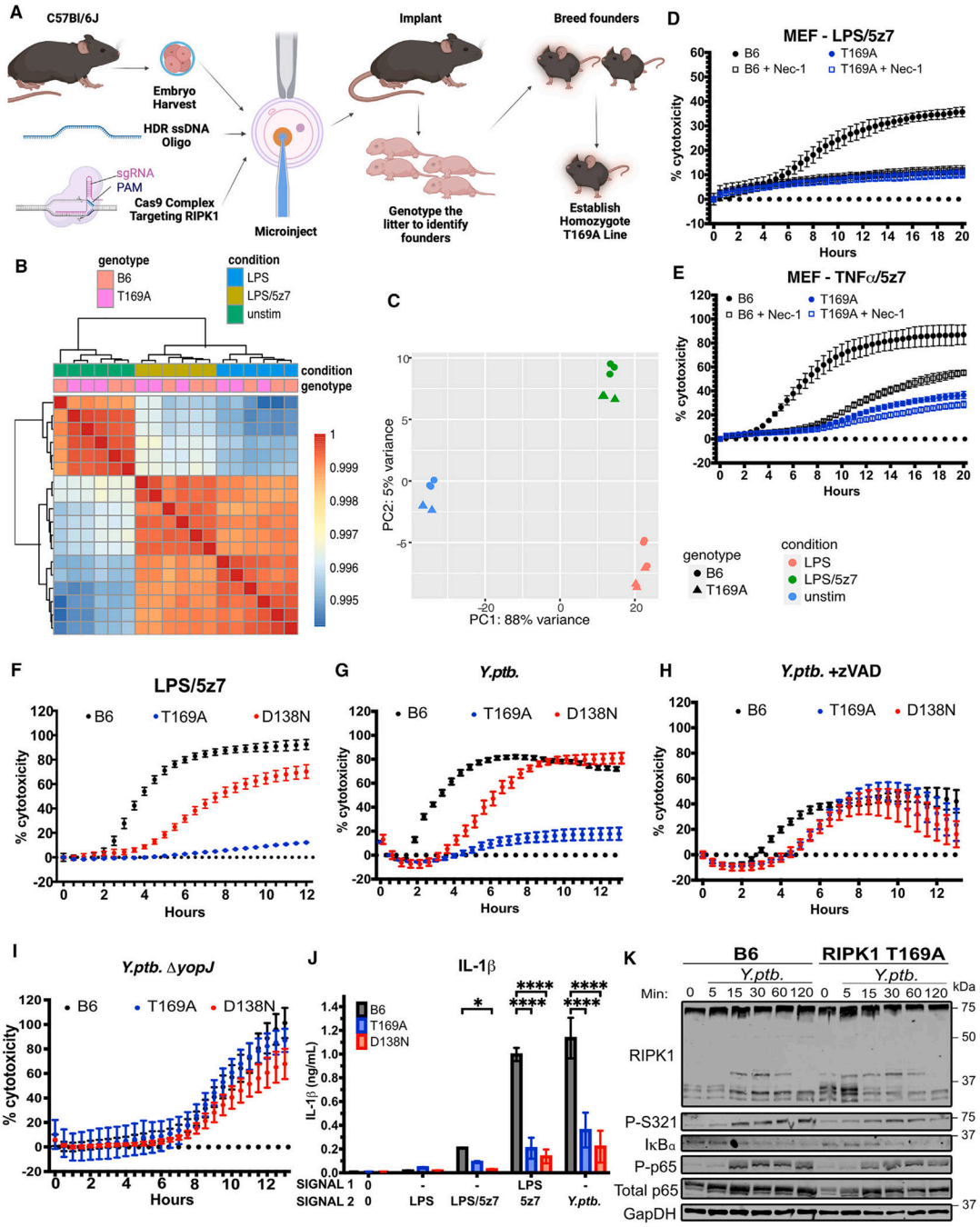

Figure 2. Inhibition of RIPK1 T169 phosphorylation inhibits CASP8-dependent death and downstream pyroptosis without altering inflammatory signaling

(A) Schema depicting the establishment of the *Ripk1*$^{T169A/T169A}$ mouse line created in BioRender.

(B) Sample-sample correlation heatmap of B6 and RIPK1 T169A BMDMs treated with LPS, LPS/5z7, or unstimulated. $N = 3$ for each genotype and stimulation.

(C) Principal-component analysis (PCA) plot of bulk RNA sequencing analysis of B6 and RIPK1 T169A BMDMs treated with LPS or LPS/5z7 or unstimulated. $N = 3$ for each genotype and stimulation.

(D–I) Cell death as measured by PI incorporation over time in (D and E) B6 and RIPK1 T169A MEFs or (F–I) B6, RIPK1 T169A, and RIPK1 D138N primary BMDMs stimulated with (D and F) LPS/5z7, (E) TNF-α/5z7, (G and H) *Y. ptb.* at an MOI of 12, or (I) ΔYopJ-deficient *Y. ptb.* at an MOI of 12, respectively.

(J) IL-1β release from B6, RIPK1 T169A, and RIPK1 D138N primary BMDMs after 16 h of indicated treatments. LPS priming (10 ng/mL) occurred 4 h before the addition of 5z7.

(K) Western blot for GapDH, RIPK1, RIPK1 phospho-S321, total IκBα, NF-κB phospho-p65, and NF-κB total p65 in B6 and RIPK1 T169A BMDMs stimulated with *Y. ptb.* at MOI of 12 over indicated time.

Data from cell death assays and western blots are representative of 3 or more biologically independent experiments, cell death data are presented as the mean ± SD of triplicate wells, and $n = 10{,}000$ cells examined in three individual wells. IL-1β release data are presented as the mean ± SD for triplicate wells from $n = 3$ independent biologic experiments. Two-way ANOVA was used for comparison between groups: ns, non-significant ($p > 0.05$), *$p < 0.05$, **$p < 0.01$, ***$p < 0.001$, and ****$p < 0.0001$.

See also Figure S2.

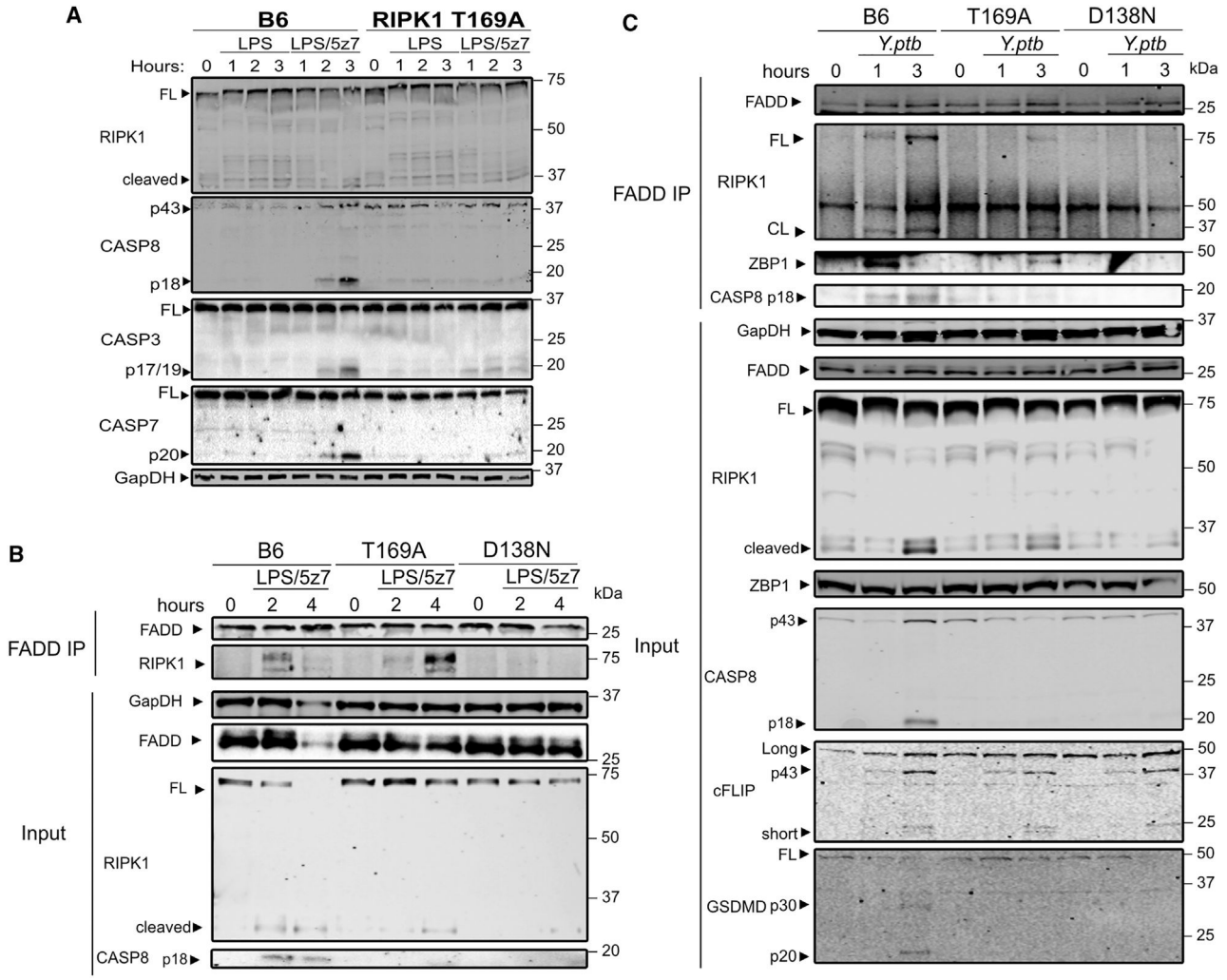

Figure 3. RIPK1 T169A BMDMs form a delayed death complex but do not induce caspase cleavage

(A) Western blot for GapDH, RIPK1, cleaved CASP8, CASP3, and CASP7 in B6 and RIPK1 T169A BMDMs stimulated with LPS or LPS/5z7 over the indicated amounts of time.

(B) FADD immunoprecipitation (IP) of B6, RIPK1 T169A, and RIPK1 D138N primary BMDMs stimulated with LPS/5z7 for 0, 2, or 4 h and probed for FADD and RIPK1. Inputs were probed for GapDH, FADD, RIPK1, and cleaved CASP8.

(C) FADD IP of B6, RIPK1 T169A, and RIPK1 D138N primary BMDMs stimulated with *Y.ptb*. for 0, 1, and 3 h and probed for FADD, ZBP1, and RIPK1. Inputs were probed for GapDH, FADD, RIPK1, ZBP1, cleaved CASP8, cellular FLICE-like inhibitory protein (cFLIP), and GSDMD.

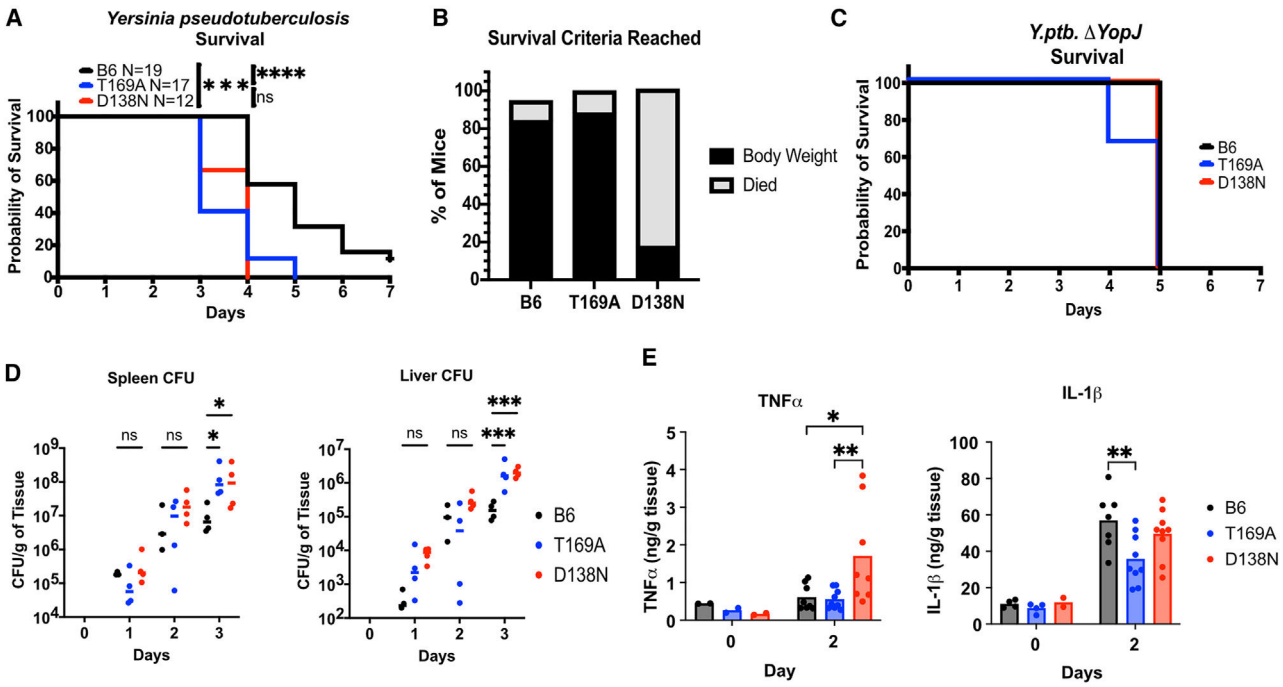

Figure 4. RIPK1 T169A mice are more susceptible to *Y.ptb. in vivo*, corresponding to a decrease in splenic IL-1β during early infection

(A) Kaplan-Meir survival curve of 8- to 10-week-old B6, T169A, and D138N mice treated with 5×10^2 CFUs of *Y.ptb.* via intravenous (i.v.) injection.

(B) Percentage of mice that reached the 85% of original body weight sacrifice criterion or experienced spontaneous death across all mice in (A).

(C) Kaplan-Meir survival curve of 8- to 12-week-old B6, T169A, and D138N mice treated with 5×10^2 CFUs of *Y.ptb.* deficient for YopJ via i.v. injection. $N = 3$.

(D) Spleen and liver CFUs for mice sacrificed on the indicated day post-infection. For each time point and genotype, $N = 4$.

(E) TNF-α and IL-1β protein levels measured by ELISA in the spleen of B6, T169A, and D138N mice injected i.v. with *Y.ptb.* for the indicated amounts of time. For PBS mice, $N = 2–4$ mice per genotype. For 2-day infected mice, $N = 8–9$ mice per genotype. Log-rank (Mantel-Cox) test was used for comparison of survival curves.

Two-way ANOVA was used for comparison between groups: ns, non-significant ($p > 0.05$), *$p < 0.05$, **$p < 0.01$, ***$p < 0.001$, and ****$p < 0.0001$.

See also Figure S3.

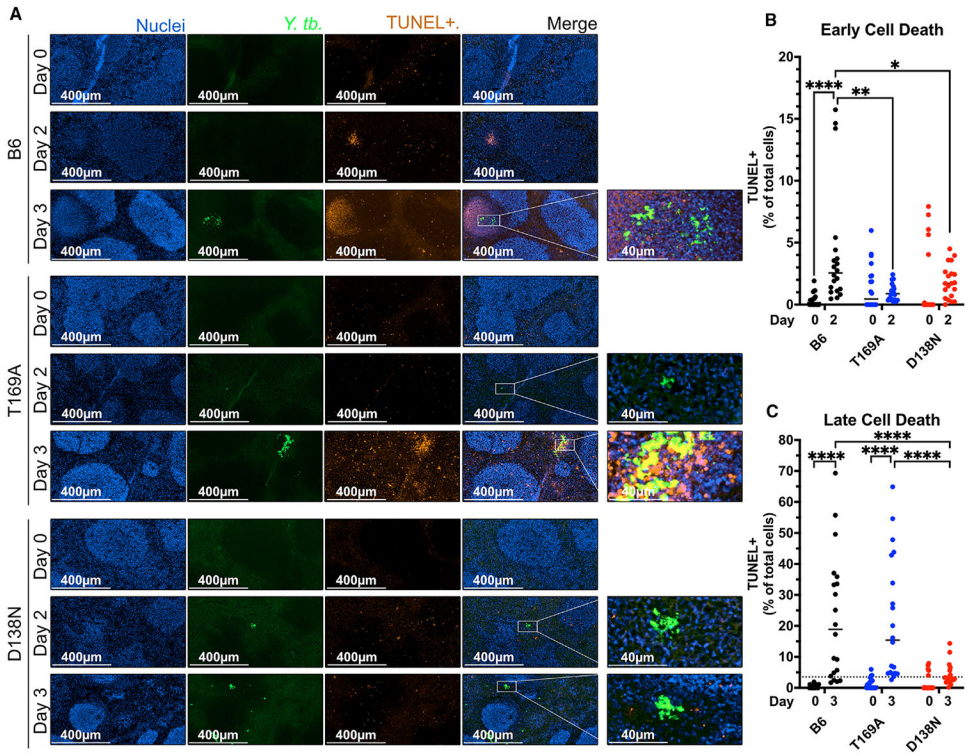

Figure 5. RIPK1 T169A mice experience delayed onset of cell death in the spleen after early *Y.ptb*. foci formation that rapidly increases to levels similar to those seen in B6 mice

(A) TUNEL staining and (B and C) quantification of percentage of total cells that are TUNEL+ in the spleens of B6, RIPK1 T169A, and RIPK1 D138N mice injected i.v. with GFP+ *Y.ptb.* for the indicated times. DAPI, 4′,6-diamidino-2 phenylindole. Each point represents one field of view, with a total of 5 fields of view across four biological replicates. Two-way ANOVA was used for comparison between groups: ns, non-significant ($p > 0.05$), *$p < 0.05$, **$p < 0.01$, ***$p < 0.001$, and ****$p < 0.0001$.

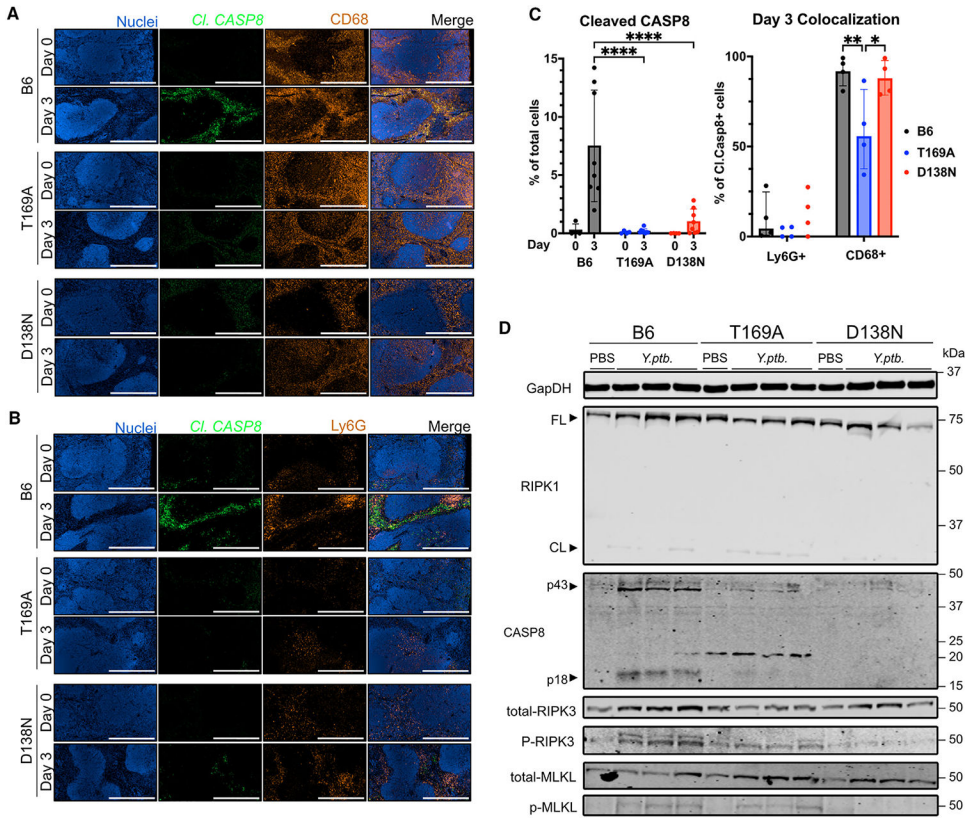

Figure 6. RIPK1 T169A mice activate p-MLKL, and not CASP8, in the spleen during *in vivo Y.ptb*. infection

(A and B) Immunofluorescence staining for cleaved CASP8 and (A) CD68 or (B) Ly6G in the spleens of B6, RIPK1 T169A, and RIPK1 D138N mice injected i.v. with *Y.ptb.* for 0 or 3 days. DAPI, 4′,6-diamidino-2 phenylindole. All scale bars shown represent 400 μm.

(C) Quantification of (A) and (B) for percentage of total cells that are cleaved CASP8+ in the spleens of B6, RIPK1 T169A, and RIPK1 D138N mice and quantification of cleaved CASP8+ colocalization with either CD68 or Ly6G. Each point represents one tissue field of view across four biological replicates. Two-way ANOVA was used for comparison between groups: ns, non-significant ($p > 0.05$), *$p < 0.05$, **$p < 0.01$, ***$p < 0.001$, and ****$p < 0.0001$.

(D) Western blot of spleen lysates from B6, RIPK1 T169A, and RIPK1 D138N mice i.v. injected with either PBS or *Y.ptb.* for 3 days as indicated probed for GapDH, cleaved CASP8, GSDMD, phospho-RIPK3 and total RIPK3, and phospho-MLKL and total MLKL. Data from western blots are representative of 4 or more biological replicates for each indicated treatment.

KEY RESOURCES TABLE

REAGENTor RESOURCE	SOURCE	IDENTIFIER
Antibodies		
CD68	BioRad	Cat#: MCA1957; RRID: AB_322219
Ly6G	BD Biosciences	Cat#: 551459; RRID: AB_394206
Goat anti-Rabbit IgG Alexa Fluor 488	Invitrogen	Cat#:A21202; RRID: AB_141607
Goat anti-Rat IgG Alexa Fluor 555	Invitrogen	Cat#: A21434; RRID: AB_2535855
RIPK1	Cell Signaling Technology	Cat#: 3493; RRID: AB_2305314
RIPK1 p-S166	Cell Signaling Technology	Cat#: 31122; RRID: AB_2799000
Caspase 3	Cell Signaling Technology	Cat#: 9662; RRID: AB_331439
Caspase 7	Cell Signaling Technology	Cat#: 9492; RRID: AB_2228313
cleaved CASP8	Cell Signaling Technology	Cat#: 8592; RRID: AB_10891784
RIPK3	Cell Signaling Technology	Cat#: 95702; RRID: AB_2721823
p-RIPK3	Cell Signaling Technology	Cat#: 91702; RRID: AB_2137060
MLKL	Millipore	Cat#: MABC604; RRID: AB_2820284
p-MLKL-S345	Abcam	Cat#: ab196436; RRID: AB_2687465
SAPK/JNK	Cell Signaling Technology	Cat#: 9252; RRID: AB_2250373
p-SAPK/JNK	Cell Signaling Technology	Cat#: 9255; RRID: AB_2307321
p38	Cell Signaling Technology	Cat#: 9212; RRID: AB_330713
p-p38	Cell Signaling Technology	Cat#: 4511: RRID: AB_2139682
ERK1/2	Cell Signaling Technology	Cat#: 4696; RRID: AB_390780
p-ERK1/2	Cell Signaling Technology	Cat# 4370: RRID: AB_2315112
GAPDH	Cell Signaling Technology	Cat#: 2118; RRID: AB_561053
FADD	Millipore Sigma	Cat#: 05-486; RRID: AB_ 2100627
ZBP1 (Zippy)	Adipogen	Cat#: AG-20B-0010-C100; RRID: AB_2490191
RIPK1	BD Biosciences	Cat#: 610458; RRID: AB_397831
GSDMD	Abcam	Cat#: Ab209845; RRID: AB_2783550
RIPK1- pS321	Cell Signaling Technology	Cat#: 38662; RRID: AB_3094762
IκBα	Cell Signaling Technology	Cat#: 4812; RRID: AB_10694416
NF-κB p-p65	Cell Signaling Technology	Cat#: 3033; RRID: AB_331284
NF-κB p65	Cell Signaling Technology	Cat#: 8242; RRID: AB_10859369
cFLIP Cell Signaling Technology		Cat#: 56343; RRID: AB_2799508
anti-rabbit IgG (H + L) (DyLight™ 800 4X PEG Conjugate)	Cell Signaling Technology	Cat#: 5151; RRID: AB_10697505
anti-mouse IgG (H + L) (DyLight™ 800 4X PEG Conjugate)	Cell Signaling Technology	Cat#: 5257; RRID: AB_10693543
Bacterial and virus strains		
Yersinia pseudotuberculosis IP2666	Ralph Isberg	N/A
Yersinia pseudotuberculosis IP2666 ΔYopJ	Ralph Isberg	N/A
Yersinia pseudotuberculosis IP2666 GFP+	Ralph Isberg	N/A
Chemicals, peptides, and recombinant proteins		

REAGENTor RESOURCE	SOURCE	IDENTIFIER
Bio Safe Coomassie G250 stain	Biorad	1610786
Propidium iodide	Invitrogen	P3566
Hoechst	ThermoFisher	62249
Alt-R Cas9 Electroporation Enhancer	IDT	1075915
Alt-R HDR Enhancer V2	IDT	10007910
Alt-R S.p. Cas9 Nuclease V3	IDT	1081058
Alt-R CRISPR-Cas9 tracrRNA	IDT	1072532
LPS Escherichia coli 011: B4	Sigma Aldrich	L4391
5Z-7-Oxozeaenol (5z7)	Sigma Aldrich	O9890
Necrostatin-1	Sigma Aldrich	N9037
GSK'872	Sigma Aldrich	530389
Critical commercial assays		
Murine TNF ELISA kit	R&D Systems	DY410
Murine IL1 β ELISA kit	R&D Systems	DY401
Murine CXCL1 ELISA kit	R&D Systems	DY453
Murine IL-6 ELISA kit	R&D Systems	DY406
In Situ Cell Death Detection Kit, TM Texas Red	Roche	12156792910
Deposited data		
Gene Expression Omnibus	This paper	GEO: GSE263905
Experimental models: Cell lines		
BMDM Cells: C57BL/6J	Jackson Laboratory	JAX: 000664
BMDM Cells: Balb/c	Jackson Laboratory	JAX: 000651
BMDM Cells: *Ripki*^{D138ND138N}	Dr. M. Kelliher	N/A[13]
BMDM Cells: *Ripk1*^{Tle9Ame9A}	This paper	N/A
BMDM Cells: Immortalized C57BL/6J	Dr. K. Fitzgerald	N/A
MEF Cells: C57BL/6J	Jackson Laboratory	JAX: 000664
MEF Cells: *Ripk1*$^{Tle9A/Tle9A}$	This paper	N/A
Experimental models: Organisms/strains		
Mouse: C57BL/6J	Jackson Laboratory	JAX: 000664
Mouse: *Ripki*^{D138ND138N}	Dr. M. Kelliher	N/A[13]
Mouse: *Ripk1*$^{Tle9A/Tle9A}$	This paper	N/A
Oligonucleotides		
Alt-R CRISPR-Cas9 crRNA Target sequence for generation of D138N: 5′ TGA CAA AGG TGT GAT ACA CA 3′	IDT	CD.HC9.JJB0317.AL
Alt-R CRISPR-Cas9 crRNA Target sequence for generation of S166A or T169A: 5′ GAC ATG GAG CAA ACT GAC TA3′	IDT	CD.HC9.VNMJ0917.AH

REAGENTor RESOURCE	SOURCE	IDENTIFIER
ssODN rapair oligo for generation of D138N iBMDM: IDT 5′ ATA GAA GGC ATG TGC TAC TTA CAT GAC AAA GGT GTG ATA CAC AAG AAC CTG AAG CCT GAG AAT ATC CTC GTT GAT CGT GAC TTT CA 3’		N/A
ssODN rapair oligo for generation of S166A iBMDM: 5′ TCT TTT CCA GAT AGC CGA TCT TGG TGT GGC TTC CTT TAA GAC ATG GGC CAA ACT GAC TAA GGA GAA AGA CAA CAA GCA GAA AGA AGT GA 3′.	IDT	N/A
ssODN rapair oligo for generation of T169A iBMDM: 5′ CGA TCT TGG TGT GGC TTC CTT TAA GAC ATG GAG CAA ACT GGC TAA GGA GAA AGA CAA CAA GCA GAA AGA AGT GAG CAG CAC CA 3′	IDT	N/A
ssODN rapair oligo for generation of T169A mouse: 5′ CGA TCT TGG TGT GGC TTC CTT TAA GAC ATG GAG CAA ACT GGC CAA GGA GAA AGA CAA CAA GCA GAA AGA AGT GAG CAG CAC CA 3′	IDT	N/A
Forward primer for sequencing genomic DNA of D138N mutant: 5’ TAT ATT TCA CCA TTT TCT CCT TCC C 3’	IDT	N/A
Reverse primer for sequencing genomic DNA of D138N mutant: 5’ GGA AAC AAA ACC CAG GAA CC 3’	IDT	N/A
Forward primer for sequencing genomic DNA of S166A and T169A mutant: 5’ GGT TAT CTT TCT CTG CCT TTA TGT G 3’	IDT	N/A
Reverse primer for sequencing genomic DNA of S166A and T169A mutant: 5’ TGT CTT ACT CTC ATA GGG CTC C 3’	IDT	N/A
Software and algorithms		
Prism 10	GraphPad	N/A
Gen5 Image Prime 3.10	Agilent	N/A
TrimGalore	Altos Labs	N/A
STAR	Dobin et al.[45]	N/A
FeatureCounts	Liao et al.[46]	N/A
DESeq2	Bioconductor	N/A